SUPPLEMENTARY METHODS

1.1 EMG RECORDINGS & ANALYSIS

Electromyography

We used two four-prong electrodes (a bipolar pair per muscle) constructed from 0.04 or 0.08 in. diameter tungsten rods (A-M Systems, Sequim, WA, USA), attached to insulted 0.005 in. silver wire (A-M Systems) with conductive epoxy and formed into a bundle using non-conductive epoxy with a geometry specific to recording from the DLMs and DVMs. Moths were restrained using brief (10 min.) cold anesthetization, if necessary to reduce activity. The DVM electrodes were inserted ventrally at the muscles' insertion in the medial ridge between the meso- and prothoracic legs. The DLM electrodes were inserted dorsally with one prong of each bipolar pair in the anterior region of the scutum and one in the postnotum [1]. Electrodes were held in place with a beeswax/mineral oil mixture. We placed a common mode reference electrode in the second abdominal segment that was used for all EMG channels. Data was collected at 100x amplification on differential amplifiers (A-M Systems models 1700 and 1800) at 10,000 samples*sec^{-1} with a 0.1 Hz low frequency cutoff and no line filtering. Data was acquired (National Instruments DAQ board BNC-6229 Austin, TX, USA) and captured using MATLAB (MathWorks, Natick, MA) and its data acquisition toolbox.

In one case (animal E), one muscle's EMG was lost and so we only considered one pair of muscles. In all cases, moths were dark adapted for at least 30 minutes prior to experimentation. Following this, each animal was affixed to a rigid tether. Flight occurred spontaneously or was elicited with brief tactile stimulation of the neck region. No recordings were performed while contact was made with the animal. Moths were allowed to warm-up [2] for at least two minutes during which wingstroke amplitude and frequency (judged by the period

between EMG spikes) increased visibly. Only trials where wingstroke frequency was greater than 17 Hz were considered. Wingstroke frequency was 20.9 ± 2.3 Hz (mean ± s.d.) across moths, which is typical of tethered preparations,and somewhat slower, although inclusive of, the 25 Hz frequency typical of free flight and prior workloop experiments [3].

Experiments were performed at an ambient temperature of 25°C, but following warm-up flapping, the temperature of intact moth flight muscles rises up to 10°C above ambient in tethered preps and reaches up to ~40°C in free flight stimulated preps and following warm-up flapping [2,4]. As a result, the temperatures during data collection are comparable to those used in previous, isolated muscle workloops experiments at 36°C [3].

Optomotor conditions

The refresh rate of the projector system (60 Hz) was well above the roll off frequency of the *Manduca* visual system under dark adapted conditions [5]. Spatial density (0.05 cycles*degree^{-1}) and temporal frequency (1 Hz) of the oscillating visual grating matched parameters that produced maximal responses in the moth's wide field motion sensitive neurons [5]. We monitored the visual stimulus using a small solar cell mounted to the lower, left corner of the vellum screen and measured the stimulus period during the sine trials to be 1.03 sec. due to image processing delays in rendering the video. We used this observed stimulus period in all our analyses. Only experiments where the moth visibly tracked the sinusoidal stimulus via head and abdominal bending were collected.

Spike detection methodology

Each muscle spike was discriminated off-line using threshold crossing. We visually

confirmed spike detection and ignored wingstrokes where the feature used to discriminate a spike was not consistent with other wingstrokes in the trials (e.g. the threshold level missed the first rising edge of the spike, but caught a secondary peak) or where a spike was not detected in one of the muscles. These events usually happened when the moth either slowed to a wingbeat frequency below 17 Hz or struggled its limbs, rather than the normal flight posture with legs tucked against the body. To ensure that our method of spike detection did not impact our conclusions, we confirmed our results by reanalyzing a subset of trials from several animals using peak detection methods rather than threshold crossing.

The absolute mean, but not the variance, of the left-right timing difference depended on the specific thresholds used. However, in all of these experiments we were primarily interested in how the left-right timing differences changed over the course of a trial and hence mean time differences were not important. Therefore, we subtracted the mean timing differences of each flight bout to make trials comparable.

While DLMs typically had only a single muscle potential per wingstroke for the wingstroke frequencies used in these experiments, the DVMs often had multiple spikes. In the case of multiple DVM spikes, the first spike of the burst was used. The deformation of the thorax during the wingstroke frequently induces motion artifacts in the EMG signal. To eliminate the possibility that this motion was the source of the time differences and to aid in spike discrimination, EMG traces were bandpass filtered (butterworth, 4th order) from 50-5000 Hz prior to spike detection. We replicated our results on unfiltered data in several cases and found that the difference in 98% timing windows changed by less than 0.1 ms (3.5% of the stationary and 1 to1.3% of turning trials) between the filtered and unfiltered data.

1.2 STATISTICS

Statistics were performed across all animals and on each individual as noted in the text. Equivariance, multiple group, and non-parameteric tests were implemented with JMP (SAS Institute, Inc., Cary, NC, USA). All other descriptive statistics, basic correlations, and two way tests were performed in Matlab (Mathworks, Natick, MA, USA) . Given the large number of wingstrokes analysed within each individual, normality assumptions for our within-animal parametric statistical tests could not be rejected, but when possible (*i.e.* on non-variance based tests) we confirmed our results using non parametric Kruskal-Wallis and Wilcoxon tests. Data are reported as means ± s.e.m., except for jitter measurements (standard deviations) and timing windows (98 percentiles) as noted in the text.

1.3 TORQUE MEASUREMENT & MUSCLE STIMULATION

Torquemeter & analysis

While wing kinematics are often used as measures of behavioral output, without detailed aerodynamic models it is difficult to predict how subtle changes in wing shape, rotation, or stroke will impact body dynamics, particularly in a tethered preparation [6-9]. We instead chose to measure the moth's yaw torque directly. The custom torquemeter (Fig. S2A) operates via the optical measurement of small torsional deflections of a torsionally stiff, central wire. Torque produced by the animal causes a small flag attached to the wire to move several degrees through a beam of light produced with an IR LED incident on a position sensing device (PSD). Movement of the shadow of the flag produces a voltage difference in the PSD that is processed through a custom circuit (Fig. S2B) producing an output that is proportional to the input torque. We calibrated the torquemeter using a cantilever force transducer (Fort100, WPI, Sarasota, FL)

mounted to a micromanipulation stage that deflected a small pin attached to the shaft of the torquemeter with a small protruding moment arm. Voltage was linear (Fig. S2C; $R^2 = 0.99$) with applied torque across a dynamic range larger than that observed in the experiments (±2 V).

Torque varied during each wingstroke, so we captured the mean effect by integrating torque (trapazoidal method) over the entire wingstroke. We defined a wingstroke as the time between subsequent firings of the right DLM, except in trials where the right DLM was the target of stimulation. In these cases the left DLM was used for a reference. The result of the integration of a stroke is the torque impulse (mN*mm*s). The magnitude of torque impulse produced varied from animal to animal, likely due to small errors in the alignment of the mounting pin and the yaw axis. We normalized the torque produced by each animal by finding the average torque impulse produced at the peak rightward turns of the moth during its optomotor response to the sinusoidally oscillating visual stimulus.

Muscle stimulation methods

The same electrodes were used for recording and stimulation. To encourage steady, non-turning flight so that we could test if stimulation induce turning, we used a stationary visual grating for these trials. For stimulation, EMGs were recorded from either the left or the right muscle and discriminated in realtime using a hardware voltage window discriminator (FHC Inc., Bowdoinham, ME, USA). After an adjustable delay, the output of the discriminator was used to trigger a stimulator (A-M Systems isolated pulse stimulater 2100) acting through the second pair of electrodes targeting the contralateral muscle. An initial recording was used to estimate the wingstroke period, and then the delay between spike discrimination and stimulation was set to be ~5 ms less than this period. Ideally this produced an evoked muscle potential (evoked spike) in

the contralateral muscle, 5 ms prior to where one would normally occurred. Leaving the ipsilateral muscle unaffected resulted in a 5 ms timing difference between the left and right muscles. Given the natural variability in wingstroke frequency, the induced left-right timing difference was variable and so we measured the actual timing difference in the EMG recordings post experiment (Table S1). We only accepted stimulation trials where the timing difference was less than 10 ms. We chose to advance the activity in only the left or the right muscle for each animal, because each stimulation trial provided only one data point. We collected as many trials as possible (at least 20) from each animal on one side rather than splitting our efforts between both.

We chose a stimulation pulse comparable to the *in vitro* muscle physiology experiment of Tu and Daniel (2004). Stimulation was bipolar along the longitudinal axis of the muscle (anterior to posterior in this case) and brief (0.5 ms). During stimulation, torque impulse was measured as before and compared to the immediately preceding wingstroke. Results were normalized to the turning torque found in the optomotor experiments and reported as a percentage of this turning torque.

Stimulation calibration and controls

We performed several controls to calibrate the strength of the voltage needed to produce a muscle depolarization. Quiescent animals were mounted on the torquemeter and stimulus voltage was slowly increased until the muscle twitched producing a small, measurable torque. In all animals, this twitch response was first observed between 0.5 and 1 V. However, the magnitude of the twitch response did not increase with further voltage increases because stimulation evokes an actively propagating potential across the muscle and hence needs only to

exceed a threshold rather than producing a graded response. During the actual stimulation experiments we used a stimulus of 2 V to ensure effective evoked muscle potentials. Sponberg et al. [10] used a workloop preparation to show that this type of brief, bipolar stimulation of a cockroach limb muscle produces muscle work and power output statistically indistinguishable from muscle potentials produced by neural activation. While a similar direct comparison of *in vitro* methods has not been done on *Manduca* DLMs, the fact that a very brief depolarization in these recordings produces a evoked spike that persists for several milliseconds (Fig. 5A) supports the comparability of these spikes. Regardless, the stimulation approach used here parallels that used for generation of the *in vitro* power-phase relationships of the DLMs [3,11].

To ensure that stimulus evoked spikes only advanced the timing of the muscle's spike rather than adding a second spike, we performed a control experiment where we inserted both recording and stimulus electrodes into one muscle. We found that this stimulus produces a clearly identifiable evoked potential that continued for several milliseconds after the cessation of the 0.5 ms stimulation (Fig. 5A). When an evoked spike occurred in advance of when the normal spike would be produced, the naturally occurring spike for that wingstroke did not occur, presumably because the muscle had recently been depolarized. Similar "overwriting" was found in cockroach experiments [12]. In a few trials where the naturally occurring spike occurred before the stimulus evoked spike, both depolarizations were evident. For this reason, we used no trials in which the stimulated spike followed the naturally occurring spike. In the experimental trials where one DLM was recorded and the contralateral one stimulated, the non-stimulated DLM received its normal neurally produced spike and did not show an evoked depolarization characteristic of the stimulated muscle. We therefore determined that the stimulus was well isolated to the target muscle.

SUPPLEMENTARY DISCUSSION

Elaboration on the power-phase relationships in other animals

The seminal studies by Josephson [13] showed a steep power-phase slope and submaximal power output at the *in vivo* phase of activation in the flight muscle of tettigonids (katydids). While these are synchronous flight muscles like those of *Manduca*, tettigonids are from a separate insect order demonstrating that this property may span a large diversity of flying insects (Fig. 6b). More terrestrial insects also have this property. Both the main power producing femoral extensors and the typically energy-absorbing "control" muscles in the limb of the cockroach, *Blaberus discoidalis,* operate on the steep slope of their power phase curves during running, suggesting timing feedback could drive coordinated changes in power across multiple muscles (Fig. 6c) [14]. While these insect examples indicate some generality, there are exceptions. The scallop adductor muscle operates at the peak of its power phase relationship (Fig. 6d) [15]. However, this muscle is primarily involved in escape swimming and so it is possible that there is little need for a subtle control function or that it is already controlling phase to maximize power. Alternatively, historical, functional, or physiological constraints may constrain the scallop from adopting a phase with greater control potential.

There are also vertebrate examples of power-phase relationships with steep slopes. Rat gastrocnemius operates at a phase not only far from maximum power output, but also with submaximal series elastic element efficiency and reduced overall mechanical efficiency (derived from *in vitro* work loops matching locomotor conditions in [16]). However, there is again a steep slope in power (Fig. 6e). Eels, lamprey and some fish have different steady-state phases of activation running in an anterior to posterior gradient along the body arising from different

propagation speeds of electromyographic activity and length change [17-19]. In eels, a consequence of this is that the anterior muscles operate at the peak of the power-phase relationship whereas the posterior muscles operate submaximally on the portion of the curve where the slope remains steep (Fig. 6f) [19]. However, slipjack tuna (*Katsuwonis pelamis*) activate their muscles at a relatively constant phase along their body length, which is near maximal for power production [20]. In addition to their different strategies for powering movement [20], these vertebrate swimmers likely have different steady state power-phase gains and hence may employ different timing control strategies as well.

Finally, animals performing rhythmic behaviours other than locomotion, such as respiration, circulation, and vocalization could take advantage of precision timing and a high power-phase gain to modulate output. The *Hyla* genus of calling frogs use rapid muscle contractions to produce their mating calls. Suggestively, while the phase of activation for these muscles produces high power at the onset of the call, this power falls to a submaximal level during steady-state calling (Fig. 6g) [21]. The frog seems to be capable of sustaining a phase of activation that maximizes power, but does not do so for long periods of time. As with the other examples, this relationship provides the requisite conditions for a precise neural timing strategy to enact control, although in any given case the submaximal, steep slope phase of activation may be the consequence of physiological constraints, biomechanical requirements, or even of phylogenetic history.

SUPPLEMENTARY REFERENCES

1 Eaton, J. L. 1988 *Lepidopteran anatomy*. Wiley-Interscience.

2 Heinrich, B. & Bartholomew, G. A. 1971 An analysis of pre-flight warm-up in the sphinx moth, *Manduca sexta*. *J Exp Biol* **55**, 223–239.

3 Tu, M. S. & Daniel, T. L. 2004 Submaximal power output from the dorsolongitudinal flight muscles of the hawkmoth *Manduca sexta*. *J Exp Biol* **207**, 4651–4662. (doi:10.1242/jeb.01321)

4 George, N. T. & Daniel, T. L. 2011 Temperature gradients in the flight muscles of *Manduca sexta* imply a spatial gradient in muscle force and energy output. *J Exp Biol* **214**, 894–900. (doi:10.1242/jeb.047969)

5 Theobald, J. C., Warrant, E. J. & O'Carroll, D. C. 2010 Wide-field motion tuning in nocturnal hawkmoths. *Proceedings of the Royal Society of London. Series B: Biological Sciences* **277**, 853–860. (doi:10.1098/rspb.2009.1677)

6 Willmott, A. P., Ellington, C. P. & Thomas, A. L. R. 1997 Flow visualization and unsteady aerodynamics in the flight of the hawkmoth, *Manduca sexta*. *Philos T Roy Soc B* **352**, 303–316. (doi:10.1098/rstb.1997.0022)

7 Willmott, A. P. & Ellington, C. P. 1997 The mechanics of flight in the hawkmoth *Manduca sexta*. I. Kinematics of hovering and forward flight. *J Exp Biol* **200**, 2705–2722.

8 Hedrick, T. L. & Daniel, T. L. 2006 Flight control in the hawkmoth *Manduca sexta*: the inverse problem of hovering. *J Exp Biol* **209**, 3114–3130. (doi:10.1242/jeb.02363)

9 Sane, S. P. 2003 The aerodynamics of insect flight. *J Exp Biol* **206**, 4191–4208.

10 Sponberg, S., Libby, T., Mullens, C. H. & Full, R. J. 2011 Shifts in a single muscle's control potential of body dynamics are determined by mechanical feedback. *Philos T Roy Soc B* **366**, 1606–1620. (doi:10.1098/rstb.2010.0368)

11 George, N. T., Sponberg, S. & Daniel, T. L. 2012 Temperature gradients drive mechanical energy gradients in the flight muscle of *Manduca sexta*. *J Exp Biol* **215**, 471–479. (doi:10.1242/jeb.062901)

12 Sponberg, S., Spence, A. J., Mullens, C. H. & Full, R. J. 2011 A single muscle's multifunctional control potential of body dynamics for postural control and running. *Philos T Roy Soc B* **366**, 1592–1605. (doi:10.1098/rstb.2010.0367)

13 Josephson, R. K. 1985 Mechanical power output from striated-muscle during cyclic contraction. *J Exp Biol* **114**, 493–512.

14 Ahn, A. N. & Full, R. J. 2002 A motor and a brake: two leg extensor muscles acting at the same joint manage energy differently in a running insect. *J Exp Biol* **205**, 379–389.

15 Marsh, R. L. & Olson, J. M. 1994 Power output of scallop adductor muscle during contractions replicating the *in vivo* mechanical cycle. *J Exp Biol* **193**, 139–156.

16 Ettema, G. J. 1996 Mechanical efficiency and efficiency of storage and release of series elastic energy in skeletal muscle during stretch-shorten cycles. *J Exp Biol* **199**, 1983–1997.

17 Williams, T. L., Grillner, S., Smoljaninov, V. V., Wallén, P., Kashin, S. & Rossignol, S.

1989 Locomotion in lamprey and trout: The relative timing of activation and movement. *J Exp Biol* **143**, 559–566.

18 Rome, L. C., Swank, D. & Corda, D. 1993 How fish power swimming. *Science* **261**, 340–343. (doi:10.1126/science.8332898)

19 D'août, K., Curtin, N. A., Williams, T. L. & Aerts, P. 2001 Mechanical properties of red and white swimming muscles as a function of the position along the body of the eel *Anguilla anguilla*. *J Exp Biol* **204**, 2221–2230.

20 Shadwick, R. E., Katz, S. L., Korsmeyer, K. E., Knower, T. & Covell, J. W. 1999 Muscle dynamics in skipjack tuna: timing of red muscle shortening in relation to activation and body curvature during steady swimming. *J Exp Biol* **202**, 2139–2150.

21 Girgenrath, M. & Marsh, R. L. 1999 Power output of sound-producing muscles in the tree frogs *Hyla versicolor* and *Hyla chrysoscelis*. *J Exp Biol* **202**, 3225–3237.

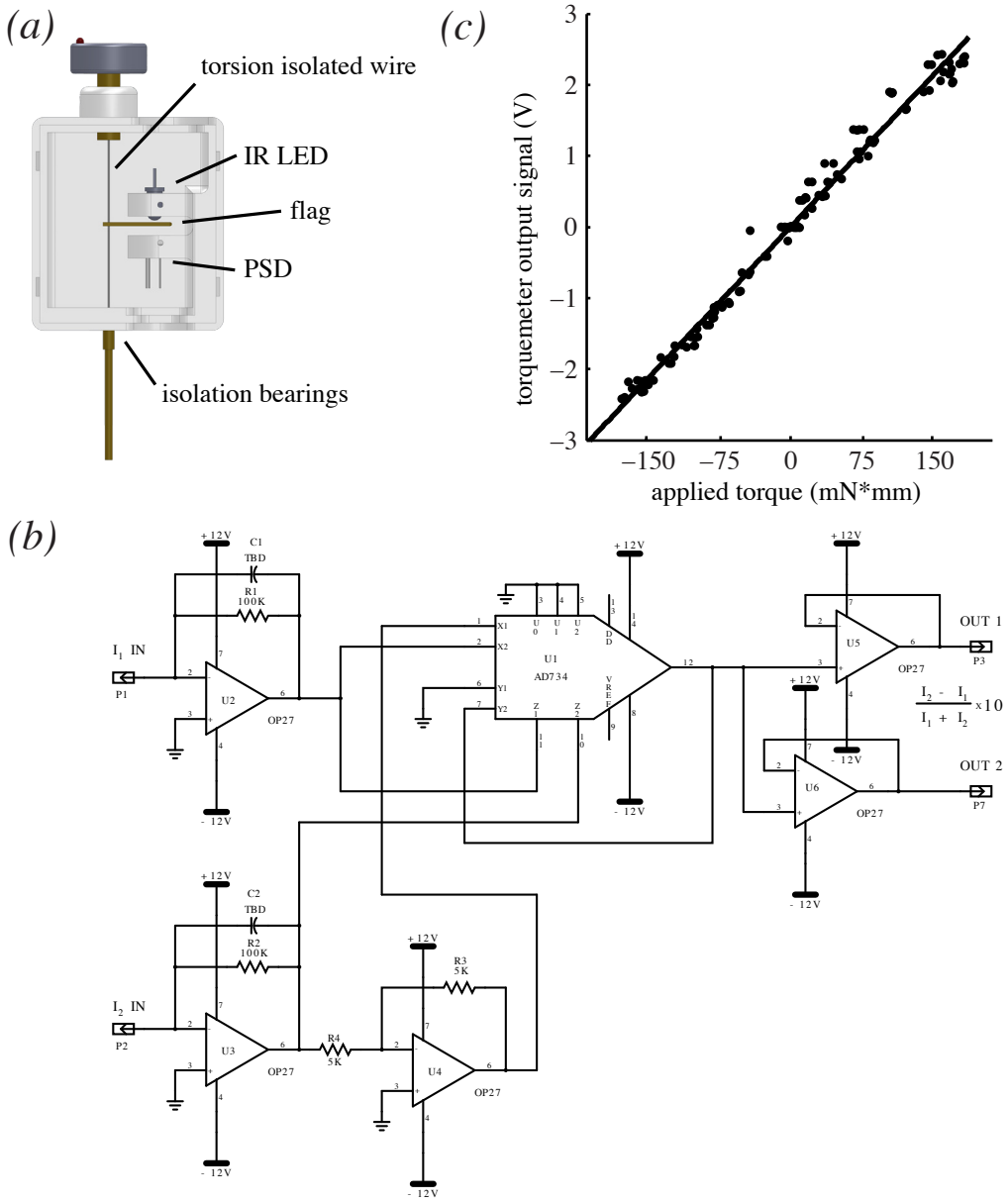

Figure S1: Torquemeter design and calibration. The optical torquemeter employs a torsionally stiff steel wire that twists approximately ± 3° in response to yaw torques typically produced by the moth (a). Isolation bearings prevent out of plane motion. A small flag is attached to the wire and passes between an IR LED and a spot 2D detector (United Detector Technologies) position sensing device (PSD). The output of two sides of the PSD are passed to two OP27s (Analog Devices) set up as transimpedance amplifiers (b). Their sum and differences are passed to an analog divide circuit (AD734) and the output is further amplified before being sent to the data acquisition board. Another op amp (U4) provides offset control for the circuit. The output voltage is linear with applied torque over a range > ± 2 V (c).

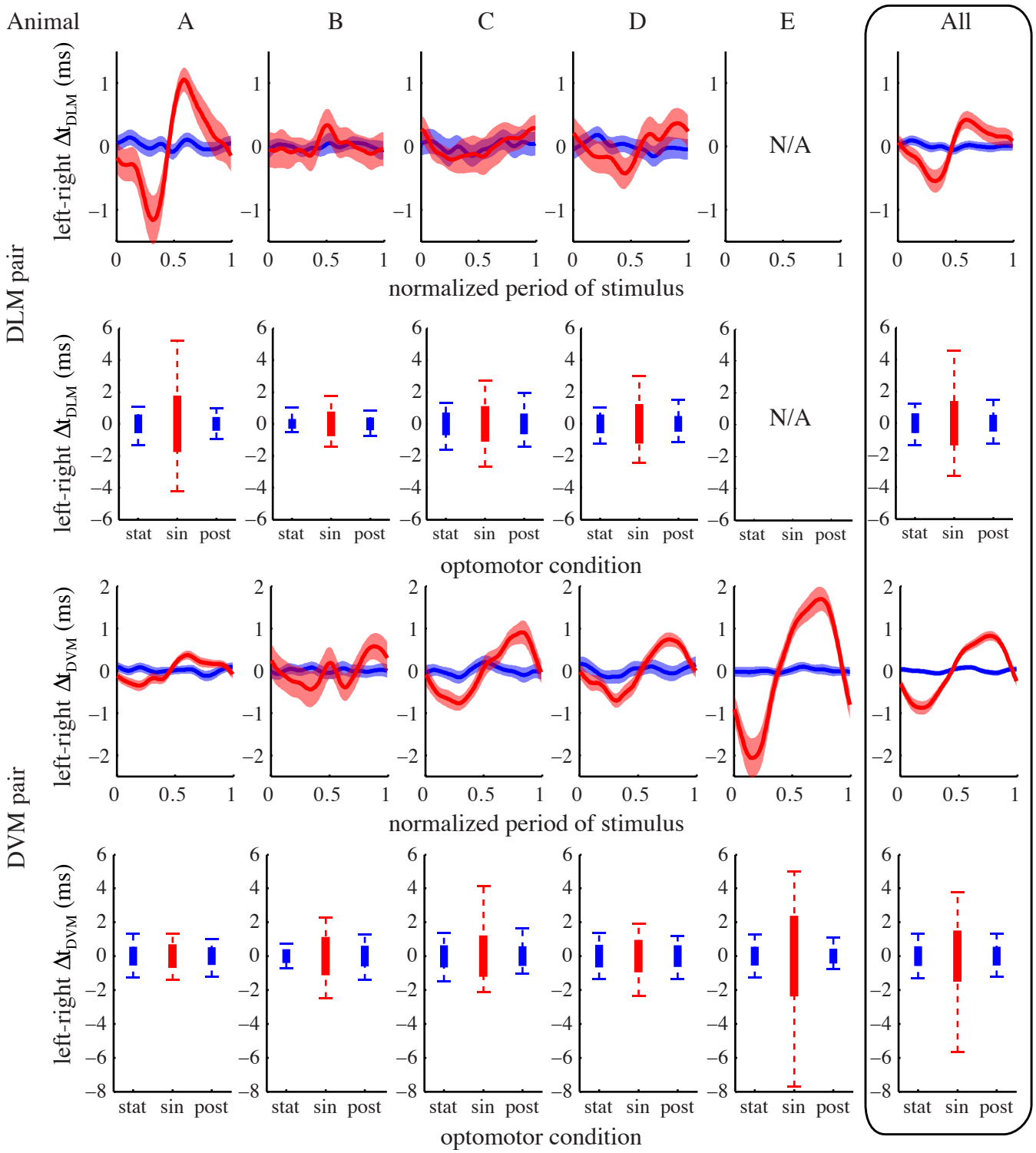

Figure S2: Individual moth DLM and DVM timing modulation during optomotor responses. Plots are the same as in figure 3, but are separated for each individual to give a sense of animal-to-animal variability. The first and third row of plots are the gaussian smoothed mean response plots for the DLMs and DVMs normalized over one period of the visual stimulus (1.03 sec.). The second and fourth rows of the plots show the jitter (standard deviation--thick bar) and 98% timing window (whiskers) in timing differences under different trial conditions as in Figure 3. While overall the DVMs showed small, but significantly greater variability than the DLMs (equivariance F-test, $P < 0.00001$), some moths demonstrated the opposite pattern (DVMs more variable than DLMs),a suggesting different individual strategies.

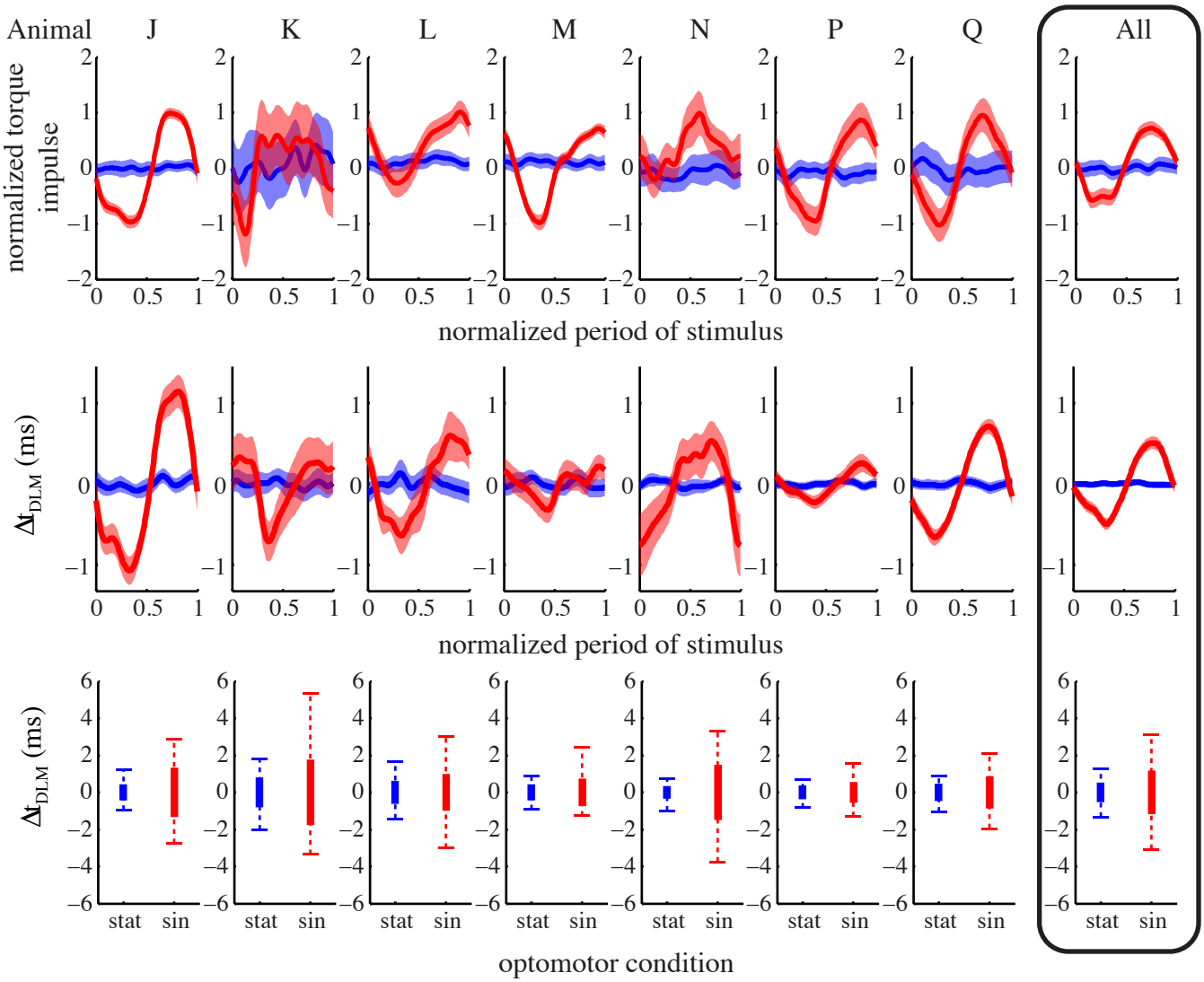

Figure S3: Individual moth torque and DLM optomotor responses. Plots are the same as in Figure 4, but are separated for each individual to give a sense of animal-to-animal variability. Top plots are the gaussian smoothed mean response plots for the normalize torque produced during the optomotor response. Middle plots are the gaussian smoothed responses for the left-right timing differences in the DLMs. The lower box plots show the variation in left-right timing under the different trial conditions in Figure 4.

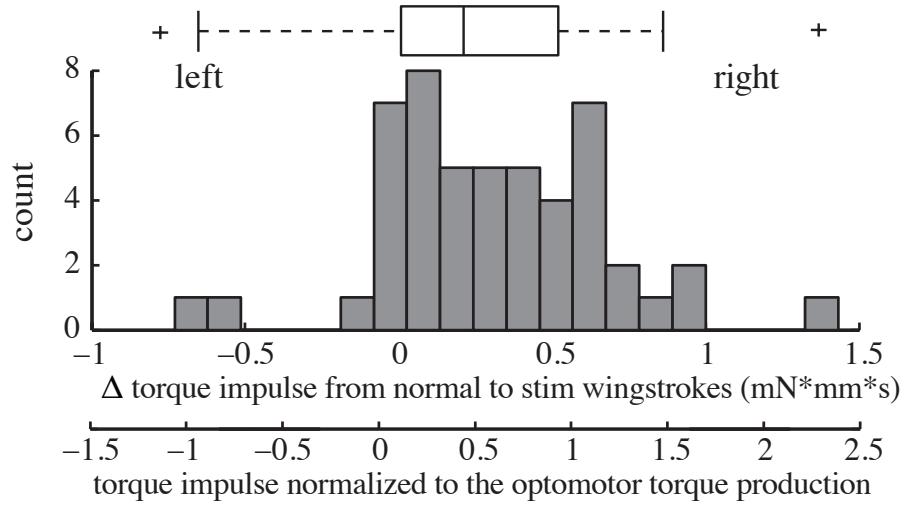

Figure S4: Torque response to induced timing differences in the DLMs in one animal (M). The histogram summarizes the responses of one moth to repeated stimulations of the right DLM, which advanced its activation ahead of the left DLM. The responses indicate mean or median increase in torque to the right indicating turning towards the stimulated side. All animals are summarized in Figure 5c and Table S1.

Supplemental Table S1: Torque response to induced phase changes in the downstroke muscle (DLM)

Animal	Q [1] (Control)	J	K	L	M	N	P	Q	All [2] (mean)	All [3] (pooled)
muscle stim side	L	R	L	L	R	R	L	L	R/L	R/L
Δt_{DLM} (ms)	0.1	2.9	-7.9	-4.1	5.3	5.8	-2.1	-3.3	4.5	4.8
jitter (ms)	0.7	1.2	2.5	2.9	3.1	2.3	1.4	2.5	2.0	2.9
% turning torque	3 ± 37	35 ± 12	-104 ± 59	5 ± 6	49 ± 8	20 ± 11	-27 ± 13	-92 ± 46	47 ± 14	37.8 ± 6
N	41	41	36	33	50	113	45	20	7	338

[1] Control trials were collected from animal Q by stimulating with the intention of inducing a $\Delta t = 0$ ms.
[2] To combine data across multiple animals the sign of the torque produced by left stim animals was flipped and combined with the right stims. This column is a mean of the animal means. N=7 animals.
[3] Same combination as above but considered across the pooled data from all animals. N=338 wingstrokes.

SUPPLEMENTARY VIDEO CAPTION

Video S1: Moth optomotor response to a visually oscillating grating. A black and white visual grating with a spatial frequency of 0.05 cycles/degree is oscillating in front of a tethered moth at 1 Hz. Active tracking of the stimulus is indicated by movement of the head, antennae and abdomen as indicated by the curved red lines demarcating the range of movement. The large red arrow indicates the direction of movement of the grating, which is off screen. This corresponds to a “sin” trial condition in the paper (Fig. 3, 4).